ALMA Memo No. 480
Thermal Properties of subsurface layer at Pampa La Bola

Seiichi Sakamoto and Hideharu Ishizaki
National Astronomical Observatory of Japan
Mitaka, Tokyo 181-8588, Japan

2004-02-06

Abstract

We monitored subsurface temperature for more than 2 years at Pampa La Bola every 20 cm down to 100 cm, and evaluated hourly temperature change, apparent thermal diffusivity, freezing points, and maximum depth to frost line. Hourly temperature changes at 0–40 cm is dominated by diurnal cycle, whereas longer timescale variation takes over at deeper layer. Annual temperature range remains 9°C peak-to-peak even at the depth of 80 cm. The hourly temperature change at 80 cm and deeper remains at a level of $\sim 0.005^\circ\mathrm{C\,hr^{-1}}$, and is mostly attributed to the annual cycle and practically cannot be overcome simply by digging deeper trenches. The apparent thermal diffusivity estimated from amplitude suppression of diurnal temperature change between 0 and 60 cm was smaller than $5.3 \times 10^{-7}\,\mathrm{m^2\,s^{-1}}$ for more than 75% of time, with the median value of $4.6 \times 10^{-7}\,\mathrm{m^2\,s^{-1}}$. A significant seasonal variation was found, with higher values (up to $\sim 10 \times 10^{-7}\,\mathrm{m^2\,s^{-1}}$) during rainy summer, and with very low values ($\sim 2 \times 10^{-7}\,\mathrm{m^2\,s^{-1}}$) in autumn and spring when freezing-thawing transition layer appears near the surface. The freezing point deduced from statistical plots was −0.2°C, and can be explained with 0.3% salinity. Annual mean subsurface temperature was higher than freezing point with slight increasing trend as a function of depth, and no permafrost will exist in the plateau. The maximum depth to the frost line is approximately 1 m at Pampa La Bola, and is estimated to be 2 m or more at Llano de Chajnantor because of lower mean temperature.

1 Introduction

Properties of subsurface layer are basic parameters for civil engineering. Among them, apparent thermal diffusivity is a key parameter to the design of the trenches for high-stability optical fibers so that their temperature change between calibration intervals could be negligible. The threshold in terms of the actual depth may differ depending on the thermal properties of the soils and rocks, and is worth measuring at the sites of interest. Even though the composition of bedrock at Pampa La Bola and Llano de Chajnantor was found to be mostly uniform through geotechnical studies [1], apparent soil thermal diffusivity may significantly vary within the Cerro Chascón science preserve as functions of location, depth, and time, since significant positional difference and time variation in soil resistivity has already been reported [2–4].

Another point of interest is frost heaving, which might degrade the performance and shorten the lifetime of ALMA antenna foundations through the activity of freeze-thaw cycle below the surface. The standard method to prevent frost heaving is to anchor the footing of foundations by building a large hole down to the frost line. For this purpose, the maximum depth to the frost line is to be measured.

To examine these thermal property of the subsurface layer at the Cerro Chascón science preserve, we started measurements of soil temperature at Pampa La Bola where the longest part of trenches for optical fibers will be located. Here we report results based on long-term (> 2 yr) measurements and compare the results with the previous ones at Llano de Chajnantor [5].

2 Measurements

The measurements have been carried out at Pampa La Bola since the end of 2000 January. A six-channel data logger (Eto Denki THERMIC 2100A) in combination with thermocouples was used to record the diurnal variation of the subsurface temperature. Relative accuracy of the thermocouples was calibrated with iced and boiled water prior to the measurements, and was proven better than 0.2°C. The probes were fixed with aluminum adhesive tape to a wooden pole so that they are appropriately located at the depths from 0 to 100 cm with a uniform spacing of 20.0 ± 0.5 cm and have sufficient thermal contact with ambient soils. The wooden pole was replaced to a grass fiber pole of better thermal insulation on 2000 June 29. Because of the continuous stiff rocks located about 60 cm in depth at the site, it was difficult to dig a deep hole (> 1 m depth) without a large rock drill. Instead, we bored a hole of about 60 cm depth and covered the rest 40 cm with the soil/rocks near the surface to simulate realistic situation expected during the actual trenching and backfilling with backhoes. Experimental setup is schematically illustrated in Figure 1. The thermocouple on the surface was shielded from direct illumination by the sun with a thin rock. Logging of the data was started a day and half after the installation of the instrument to reduce possible initial effects of the installation. The data were recorded every 20 minutes referring to the local time (UT − 4h) with the internal clock accurate to a few minutes. The data collected by 2002 April 9 were analyzed in this study. Because of readout error, however, the data from the 100 cm thermocouple were only partially taken.

3 Results and Discussion

3.1 Diurnal and Seasonal Variation of Subsurface Temperature

Time variation of the subsurface temperature is shown in Figure 2, which is combined seasonal and diurnal plots of subsurface temperature at the depths of 0, 20, 40, 60, and 80 cm. Solar radiation flux and atmospheric temperature measured with a nearby weather station (see [6] for details) during the same period were also plotted in Figure 3 for comparison. Different presentation is in Figures 4 and 5.

Time variation of the surface temperature is dominated by diurnal cycle. Typical diurnal change of the surface temperature was ∼ 30°C peak-to-peak whereas the atmospheric temperature did not show such a large amplitude of diurnal cycle (∼ 20°C peak-to-peak).

The temperature variation becomes suppressed as a function of depth. The peak-to-peak amplitude of diurnal variation at the depth after removal of longer-timescale variation was about 6°C at 20 cm, 1.5°C at 40 cm, 0.4°C at 60 cm, and 0.1°C at 80 cm, respectively. The diurnal variation at 100 cm was smaller than the temperature resolution of the system (0.1°C), and was often dominated by the variation with time constant significantly larger than 1 day.

One of the most interesting features in Figure 4 (see Figure 6 for a closer look) is thermally stable period with temperature close to 0°C observed at 60 and 80 cm during the days 560–650, followed by sudden rise of temperature ("zero curtain effect," e.g., [7]). This is also visible in Figure 7 as a local peak of the histogram near 0°C. The reason for this phenomenon is that penetration of the freezing fronts is inhibited by the release of the latent heat of fusion, and thermal fluctuations below the fronts are strongly attenuated.

There is also a delay in phase of the diurnal temperature variation as a function of depth, which is about 7 hr (1.8 radian) at 20 cm, 13 hr (3.5 radian) at 40 cm, 20 hr (5.3 radian) at 60 cm, and 27 hr (7.1 radian) at 80 cm, respectively. The diurnal variation at 100 cm was too small for the evaluation of its phase delay, and was dominated by the variation with time constant significantly larger than 1 day.

We plot in Figure 8 mean daily temperature calculated as a running mean of 24 hours for evaluation of temperature change longer than the diurnal cycle. The most severe temperature drift occurs during continuous bad weather events in autumn and just after continuous bad weather events in spring. The drift in spring is further enhanced with an onset of sudden rise of temperature due to the breakup of the zero curtain effect.

Monthly mean soil temperatures in 2001 at different depths are summarized in Table 1. The annual temperature range is 12°C peak-to-peak at 0 cm and remains 9°C at 80 cm. Annual mean soil temperature was higher than atmospheric temperature near the surface during the same period (−0.88°C). It was always higher than 0°C and increased as we go deeper, and this may also be due to the zero curtain effect. Since the mean atmospheric temperature in 2001 reasonably agrees to the one in 1997 (−0.96°C, [6]), the results of statistical analyses presented in this paper should be taken as typical ones.

3.2 Temperature Stability

Diurnal temperature profile is asymmetric — heating with smaller time constant and cooling vice versa, and this is reflected in Figure 9 as asymmetric features of hourly temperature change relative to the zero baseline. The observed maximum and median values of the largest hourly temperature change in a day on the surface were $\sim 30°\mathrm{C\,hr^{-1}}$ and $11°\mathrm{C\,hr^{-1}}$, respectively. As shown in Figure 10, which is a blow up of hourly temperature changes during the first three days of the year 2001, the largest surface temperature change occurs usually in the morning (around 8h local time) and the secondary local maximum at around 16h, with significant day-to-day variation. Because this steep rise has time constant shorter than several hours, the hourly temperature change becomes suppressed to $\sim 1.5°\mathrm{C\,hr^{-1}}$ at 20 cm (Figure 11).

At 40 and 60 cm, hourly temperature changes are dominated by sinusoidal component due to diurnal cycle, and maximum hourly temperature change at levels of $0.3°\mathrm{C\,hr^{-1}}$ at 40 cm and $0.007°\mathrm{C\,hr^{-1}}$ at 60 cm are expected from the amplitude of their respective diurnal cycles.

At 80 cm and deeper, longer timescale temperature change due to continuously bad weather conditions and annual cycle becomes significant, and the maximum hourly temperature change due to annual cycle reaches $\sim 0.005°\mathrm{C\,hr^{-1}}$ with very weak dependence on depth down to 100 cm. This value is comparable to the temperature change at 60 cm due to diurnal cycle, and thus the overall maximum hourly temperature change at 60 cm is estimated to be $\sim 0.012°\mathrm{C\,hr^{-1}}$. Because of longer timescales, this temperature variation needs far more depth to be dumped, and practically cannot be overcome.

The above results suggest that economical solution of the depth of trenches in terms of temperature stability is around 60 cm. By assuming a worst-case value of $15\,\mathrm{ppm\,K^{-1}}$ temperature coefficient for ALMA optical fibers [8], hourly length change of a 15 km fiber will not exceed $2.7\,\mathrm{mm\,hr^{-1}}$ if we bury the fiber at 60 cm depth. On the other hand, this length change is mostly attributed to the annual temperature cycle and repeats during certain seasons, and cannot be overcome simply by digging deeper trenches.

3.3 Apparent Thermal Diffusivity

3.3.1 Estimation from Amplitude Suppression and from Phase Delay

In the previous subsection, we dealt with results of direct measurements of temperature stability. Underlying physical parameters — apparent thermal diffusivity, in particular — can be deduced from the results.

There are two independent ways to estimate apparent thermal diffusivity of the subsurface layer. One is from measurements of the dumping factor of the temperature variation per unit length, and the other is from the phase delay of the temperature variation per unit length. Here we first focus on the amplitude of the temperature variation as a function of depth.

By expanding the input thermal variation with sinusoidal function, the modulation amplitude of the subsurface temperature T at the depth z and the time t is approximated as,

$$T(z,t) = T_0 + \Delta T_0 \exp[-(\omega/2\alpha')^{1/2} z] \ \sin[\omega t - (\omega/2\alpha')^{1/2} z], \tag{1}$$

where T_0 and ΔT_0 are the average temperature and the modulation amplitude of the heat cycle at the reference point, respectively, ω is the angular frequency, and α' is the apparent thermal diffusivity. We note in Equation (1) that the heat cycle with shorter timescale damps more quickly than longer one.

To avoid confusion, the term "apparent thermal diffusivity" α' is used here to indicate the values calculated from the measured temperature variations of different probe levels, instead of the term "thermal diffusivity" α, which is given as,

$$\alpha \equiv k/\rho c_p, \tag{2}$$

with the Boltzmann constant k, the mass density of the soil/rocks ρ, and the heat capacity at constant pressure c_p.

Although daily cycle is one of the dominant factors of temperature change, many Fourier components other than the daily cycle also contribute, and thus the analysis of amplitude suppression is not very straightforward. To obtain reliable values of α', following procedures have been made. Firstly, the original data were interpolated and re-sampled to have 128 samples per day. The re-sampled data were transformed with FFT algorithm and inversely transformed after removal of frequency components higher than 0.667 day^{-1}. We then removed running mean of 128 points from the data to reduce the effect of longer timescale temperature drift, and calculated the amplitude and phase of the daily cycle from the local maximum and minimum of day.

We plotted time variation of the apparent thermal diffusivity estimated from the amplitude suppression $\exp[-(\omega/2\alpha')^{1/2} z]$ in Figure 12. Median values of the apparent thermal diffusivity deduced from the 2 years data were 4.4×10^{-7} m^2 s^{-1} at 0–20 cm, 4.8×10^{-7} m^2 s^{-1} at 20–40 cm, and 5.1×10^{-7} m^2 s^{-1} at 40–60 cm, respectively (Figure 13), and showed significant seasonal and repetitive variation.

Independent estimation of the apparent thermal diffusivity is possible also from the phase delay of the cycle as a function of the depth, as shown in Equation (1). We plotted time variation of the apparent thermal diffusivity estimated from the phase delay $-(\omega/2a)^{1/2} z$ in Figure 12. Median values of the apparent thermal diffusivity were 4.4×10^{-7} m^2 s^{-1} at 0–20 cm, 4.5×10^{-7} m^2 s^{-1} at 20–40 cm, and 5.8×10^{-7} m^2 s^{-1} at 40–60 cm, respectively (Figure 13), and reasonably agree with the corresponding values estimated from the amplitude suppression in most cases.

The apparent thermal diffusivity estimated from amplitude suppression and phase delay between 0 and 60 cm had median values of 4.6×10^{-7} m^2 s^{-1} and 5.2×10^{-7} m^2 s^{-1}, respectively, and the apparent thermal diffusivity estimated from amplitude suppression fell in the range $< 5.3 \times 10^{-7}$ m^2 s^{-1} for more than 75% of time. Overall value of apparent thermal diffusivity

over 0–60 cm and over a year can be independently estimated from amplitude suppression of the annual cycle, and is consistent with the values derived from diurnal cycle above.

All of the above median values are significantly higher than the one found at Llano de Chajnantor during 1997 June–October (2.4×10^{-7} m^2 s^{-1}, [5]). We attribute this difference mostly to seasonal changes (note low values of 1–4 $\times 10^{-7}$ m^2 s^{-1} during 2001 May–October in Figure 12) as will be discussed in the next subsection, and thus the present value may better be used as representative one in the Array Operations Site.

3.3.2 Depth Dependence and Time Variation

Thermal diffusivity of soil is the ratio of the thermal conductivity of the soil to the volumetric heat capacity of the soil. The conductivity and volumetric heat capacity increase with water content so the diffusivity is also dependent upon soil water content. For mineral soils, the thermal diffusivity increases with addition of water to the pore space at low water contents. A maximum value occurs at relatively low soil moisture content ($\sim 10\%$), and then gradually decreases with increasing water content, because water has a thermal diffusivity of $1.42 \times 10^{-7}\,\mathrm{m^2\,s^{-1}}$, which corresponds to about 10% of the typical soil mineral constituents excluding quartz [9].

As shown in Figure 13, the median values of apparent thermal diffusivity fall in very narrow range of $\pm 20\%$ with very little depth dependence. This may be understood if the porosity of the subsurface layer has been homogenized through excavation and backfilling processes.

On the other hand, a significant seasonal and repetitive variation of apparent thermal diffusivity exists. One of the most outstanding features in Figure 12 is an increase of the near-surface apparent thermal diffusivity during summer up to $\sim 10 \times 10^{-7}\,\mathrm{m^2\,s^{-1}}$, probably due to the precipitation at the site. Both amplitude and phase are affected by an increase of thermal diffusivity due to additional water content as well as by direct flow of water, and these two effects in combine seem to play major roles in the enhancement of the apparent thermal diffusivity during summer.

Another feature in Figure 12 is a decrease of the apparent thermal diffusivity during fall and spring to unusually low level of $\sim 2 \times 10^{-7}\,\mathrm{m^2\,s^{-1}}$. These periods correspond to those when the frost lines lie between the probes of concern, and thus the decrease of the apparent thermal diffusivity is attributed to the zero curtain effect described in section 3.1.

3.4 Freezing Point and Frost Line

3.4.1 Freezing Point

Snyder et al. noted in their plots of the time profile of the subsurface temperature flat maxima and minima that correspond to the freezing and thawing points, respectively [5]. We also note these features in our corresponding plot in Figure 4. The freezing and thawing points deduced from statistical plots in Figure 7 were both -0.2°C, and can be explained with 30 psu (PSS-78) or about 0.3% salinity [10]. This value is significantly low compared to that measured at Llano de Chajnantor (5–8%, [5]). Assumption of very low freezing point throughout the science preserve may be misleading, and the freezing point very close to 0°C deduced from the present statistical analysis should be used for design works.

3.4.2 Permafrost and Frost Line

We note in Table 1 that the annual average layer soil temperature goes up as we go deeper and the highest temperature is always higher than the freezing point. Namely, no permafrost can exist in this area. It is thus concluded that the ice found about 1 m below the surface of Llano de Chajnantor during the geotechnical study in 2000 February is not permafrost but temporary frozen layer that will melt in a year.

At Pampa La Bola (alt. = 4800 m), the lowest temperature exceeds freezing point at around 100 cm, and thus the frost heaving of antenna foundations may be overcome if the antenna foundations are anchored at depths larger than 1 m. At Llano de Chajnantor (alt. = 5050 m), however, annual mean temperature is lower than that at Pampa La Bola by 1.8°C reflecting the 250 m height difference [6], and thus the situation on the frost heaving of antenna foundations seems a bit more complicated. Simple extrapolation with the present data suggests 2 m or more as the depth to frost line at Llano de Chajnantor.

References

[1] Geo Ambiental Consultores Ltda. 2000, "Geotechnical study, Chajnantor site, II Region," ALMA Memo 408

[2] Sakamoto, S., Ezawa, H., Takahashi, T., & Yamaguchi, N. 2000, "Vertical profile of soil resistivity at the Pampa La Bola and Llano de Chajnantor sites," ALMA Memo 326

[3] Sakamoto, S., & Sekiguchi, T. 2001, "Spatial distribution of near-surface soil resistivity in the Cerro Chascón Science Preserve," ALMA Memo 346

[4] Sakamoto, S. 2001, "Seasonal and diurnal variation of upper soil resistivity in the Cerro Chascón Science Preserve," ALMA Memo 369

[5] Snyder, L. A., Radford, S. J. E., & Holdaway, M. A. 2000, "Underground temperature fluctuations and water drainage at Chajnantor," ALMA Memo 314

[6] Sakamoto, S., Handa, K., Kohno, K., Nakai, N., Otárola, A., Radford, S. J. E., Butler, B., & Bronfman, L. 2000, "Comparison of meteorological data at the Pampa La Bola and Llano de Chajnantor sites," ALMA Memo 322

[7] Hinkel, K. M., Paetzold, F., Nelson, F. E., & Bockheim, J. G. 2001, "Patterns of soil temperature and moisture in the active layer and upper permafrost at Barrow, Alaska: 1993–1999," Global and Planetary Change, 29, 293

[8] Shillue, B. 2002, "ALMA LO distribution round trip phase correction," ALMA Memo 443

[9] de Vries, D. A. 1963, "Thermal properties of soils," in Physics of Plant Environment, ed. W. R. van Wijk (North-Holland, Amsterdam), 210

[10] Tomczak, M. 2000, Freezing Point Calculator, available at `http://www.es.flinders.edu.au/~mattom/Utilities/freeze.html`

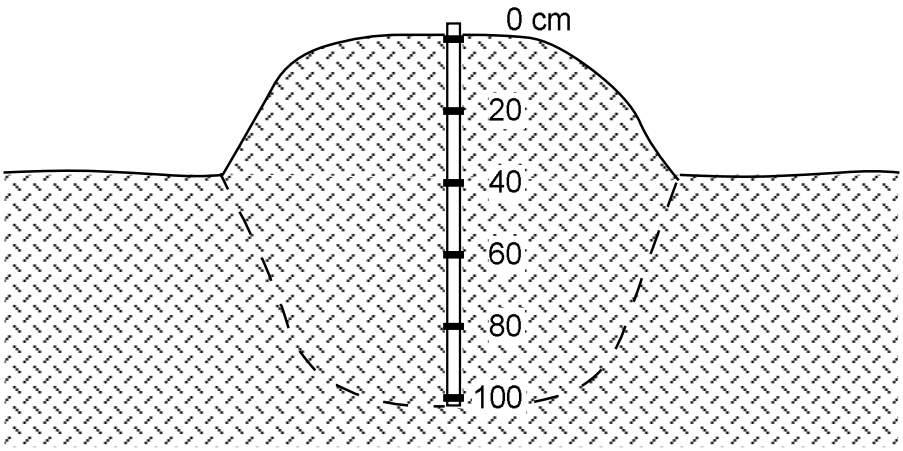

Figure 1: Experimental setup of the thermocouples. The thermocouple on the surface was shielded with a thin rock to avoid direct illumination by the sun.

Table 1: Monthly Mean Temperature of Soils and Atmosphere in 2001

Month	Mean temperature (°C)						
	atmosphere	0 cm	20 cm	40 cm	60 cm	80 cm	100 cm
Jan	2.34	7.45	8.52	8.50	8.43	8.33	...
Feb	2.93	6.96	7.70	8.00	8.09	8.13	...
Mar	1.28	4.13	5.44	5.86	6.26	6.57	6.78
Apr	0.23	2.39	3.73	4.19	4.61	4.98	5.27
May	−4.04	−3.00	−0.87	0.24	1.07	1.81	2.48
Jun	−4.13	−3.90	−2.13	−1.25	−0.45	0.24	0.75
Jul	−4.79	−4.38	−2.94	−2.16	−1.36	−0.51	0.08
Aug	−3.24	−1.90	−1.11	−0.94	−0.72	−0.40	−0.11
Sep	−2.63	0.16	0.19	−0.19	−0.29	−0.20	−0.08
Oct	−0.51	2.38	3.19	2.57	1.99	1.67	1.55
Nov	1.42	4.42	6.24	6.08	5.80	5.54	5.20
Dec	0.92	4.07	6.80	7.01	7.07	7.04	...
Mean	−0.88	1.53	2.87	3.13	3.35	3.57	...

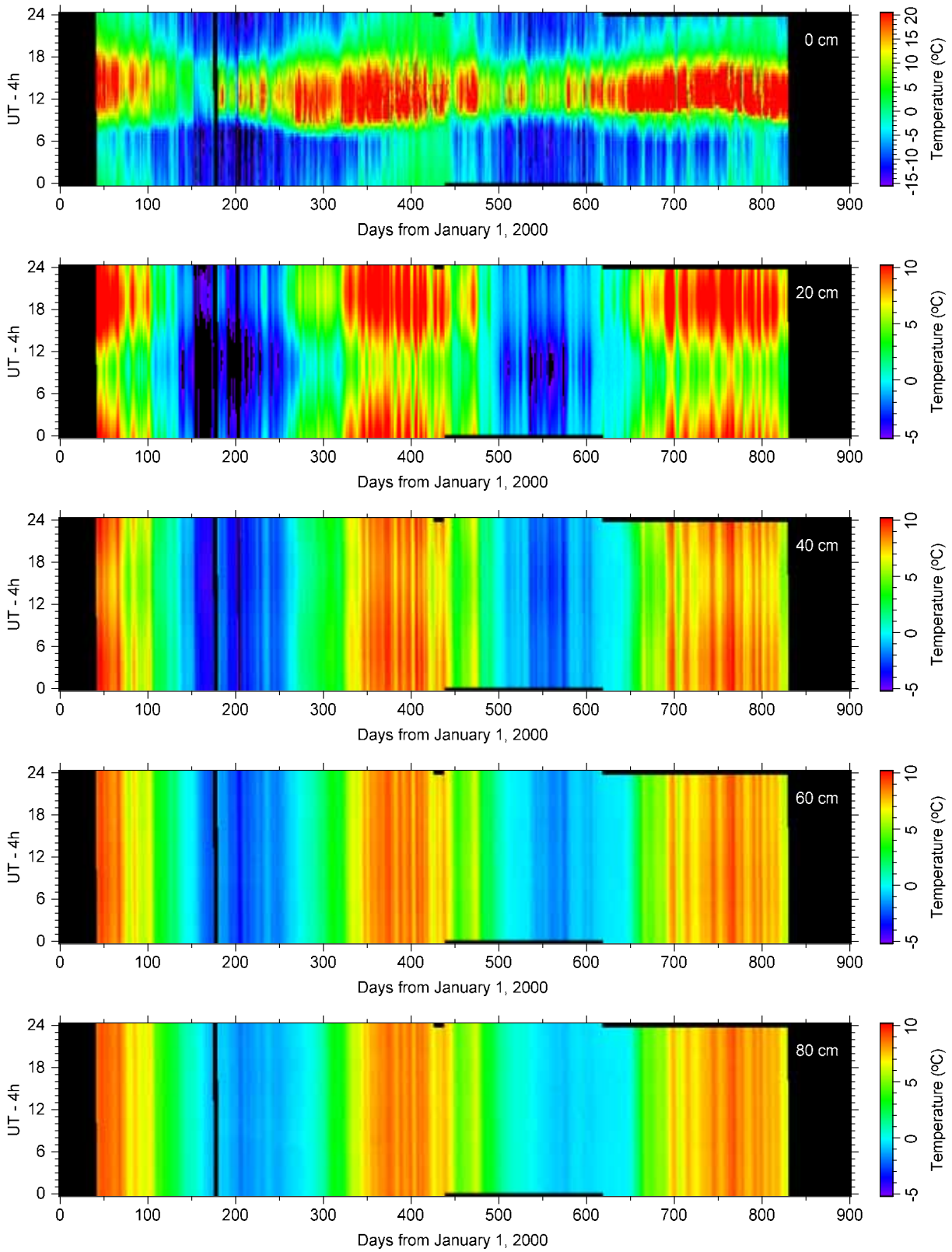

Figure 2: Combined diurnal and seasonal variation plots of temperature of subsurface layer. Note difference in color coding of the top panel.

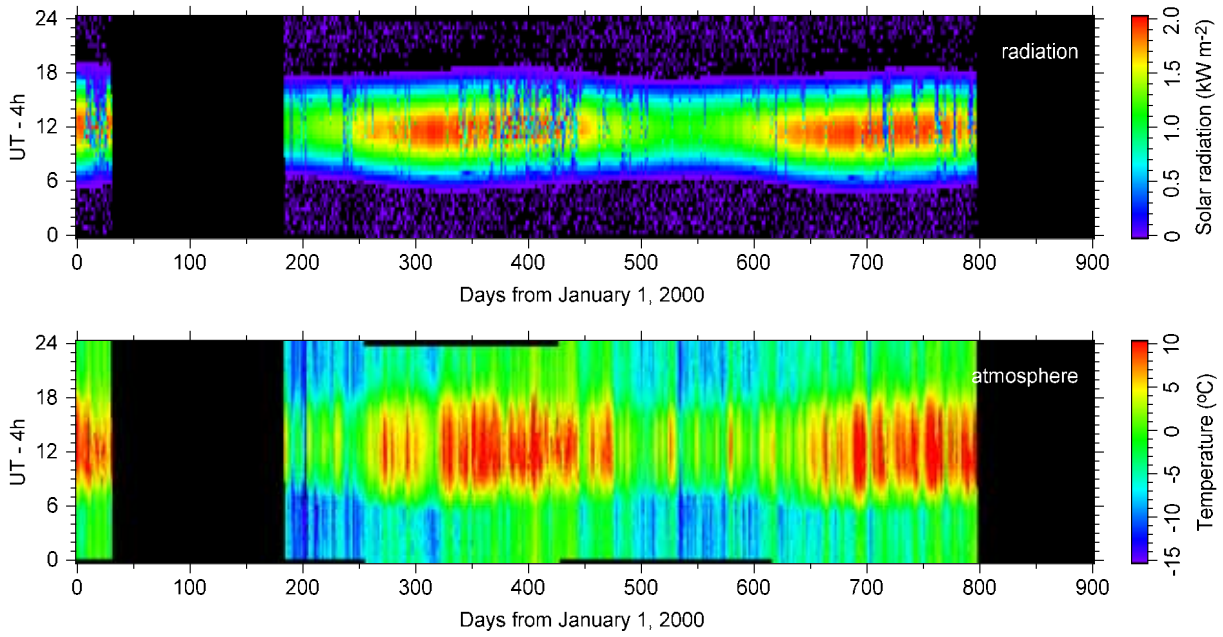

Figure 3: Combined diurnal and seasonal variation plots of solar radiation flux and atmospheric temperature taken with a nearby weather station [6].

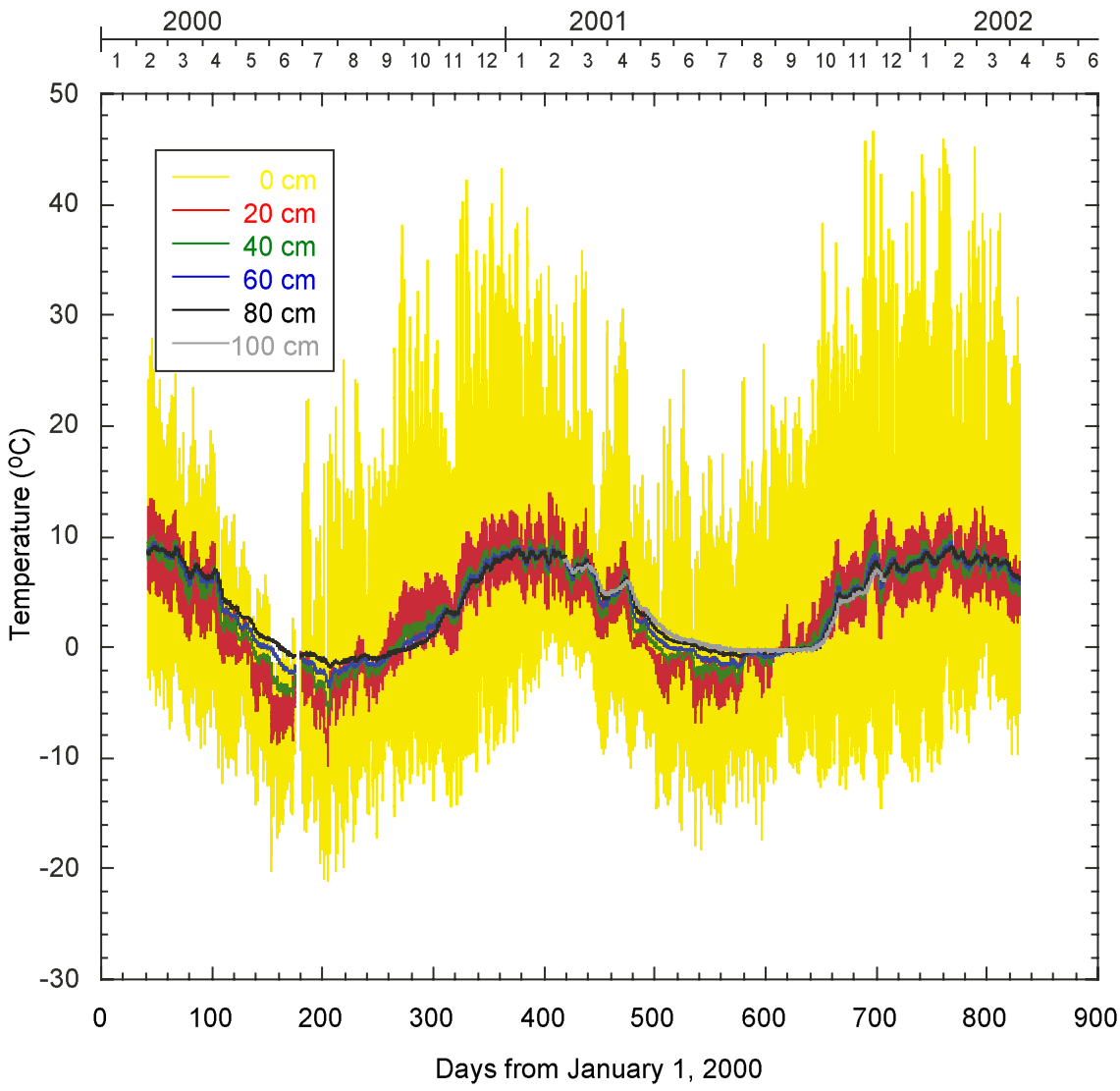

Figure 4: Time profile of temperature of subsurface layer at different depths (0, 20, 40, 60, 80, and 100 cm). Note that data taken at 100 cm depth do not cover the entire period.

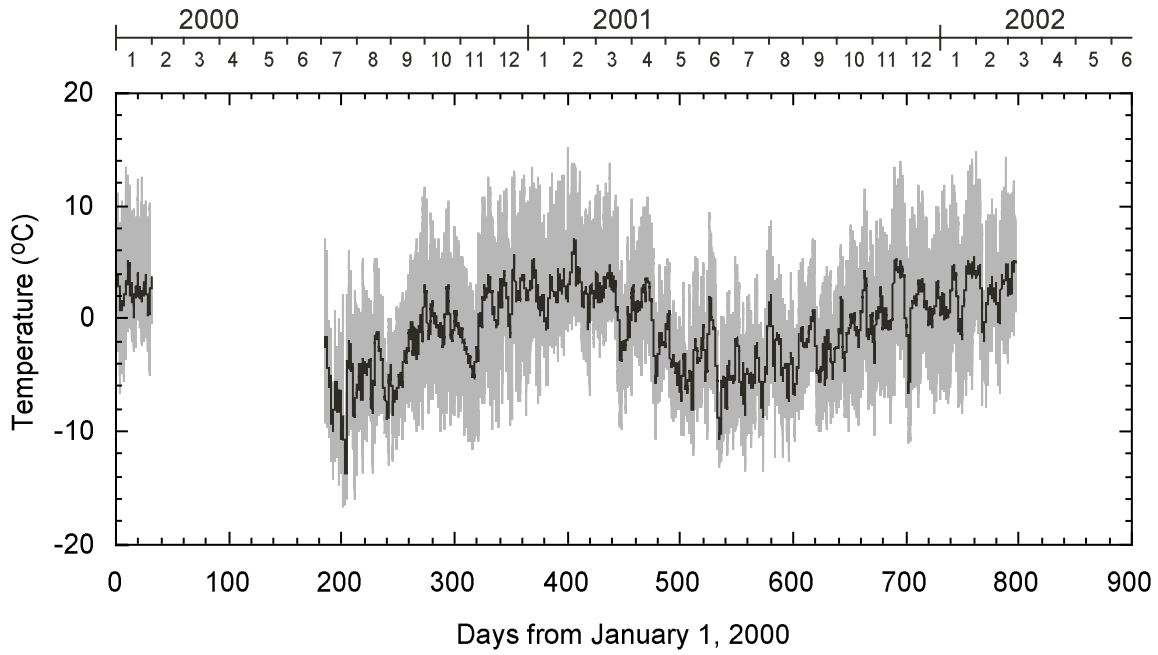

Figure 5: Time profile of atmospheric temperature and mean daily atmospheric temperature taken with a nearby weather station [6].

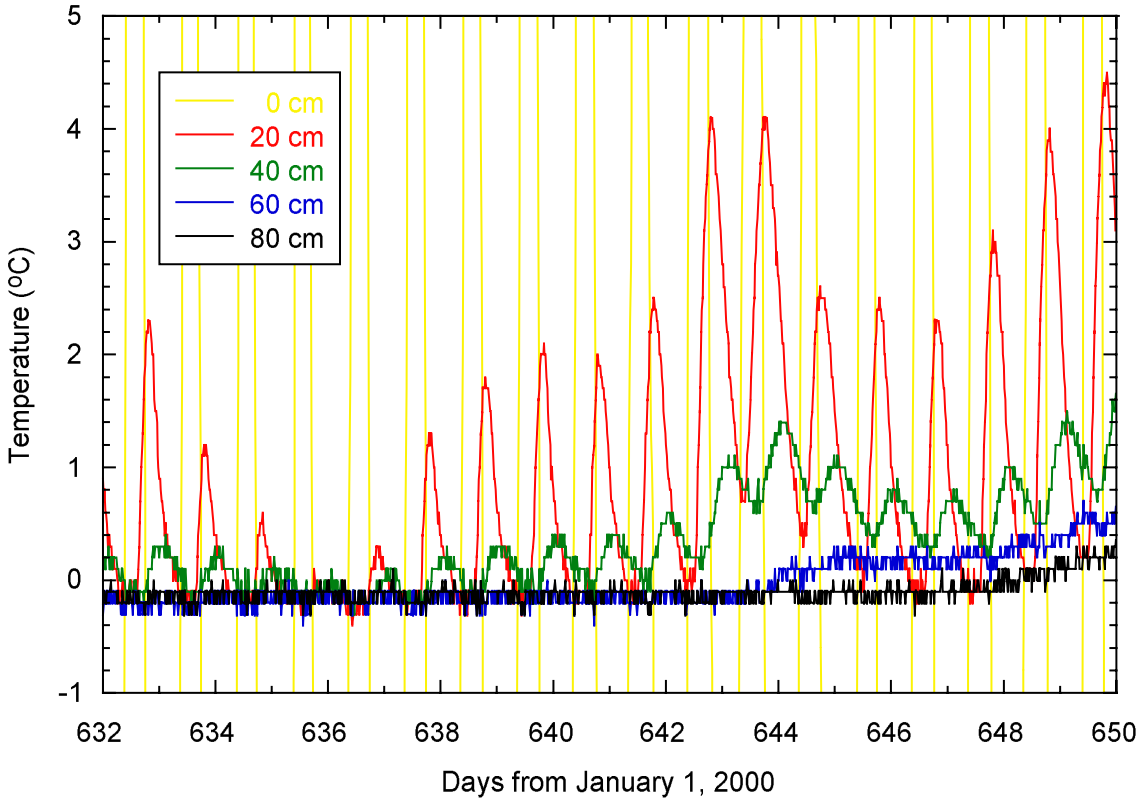

Figure 6: Same as Figure 4 but for the period between days 632 and 650, when the zero curtain effect was outstanding.

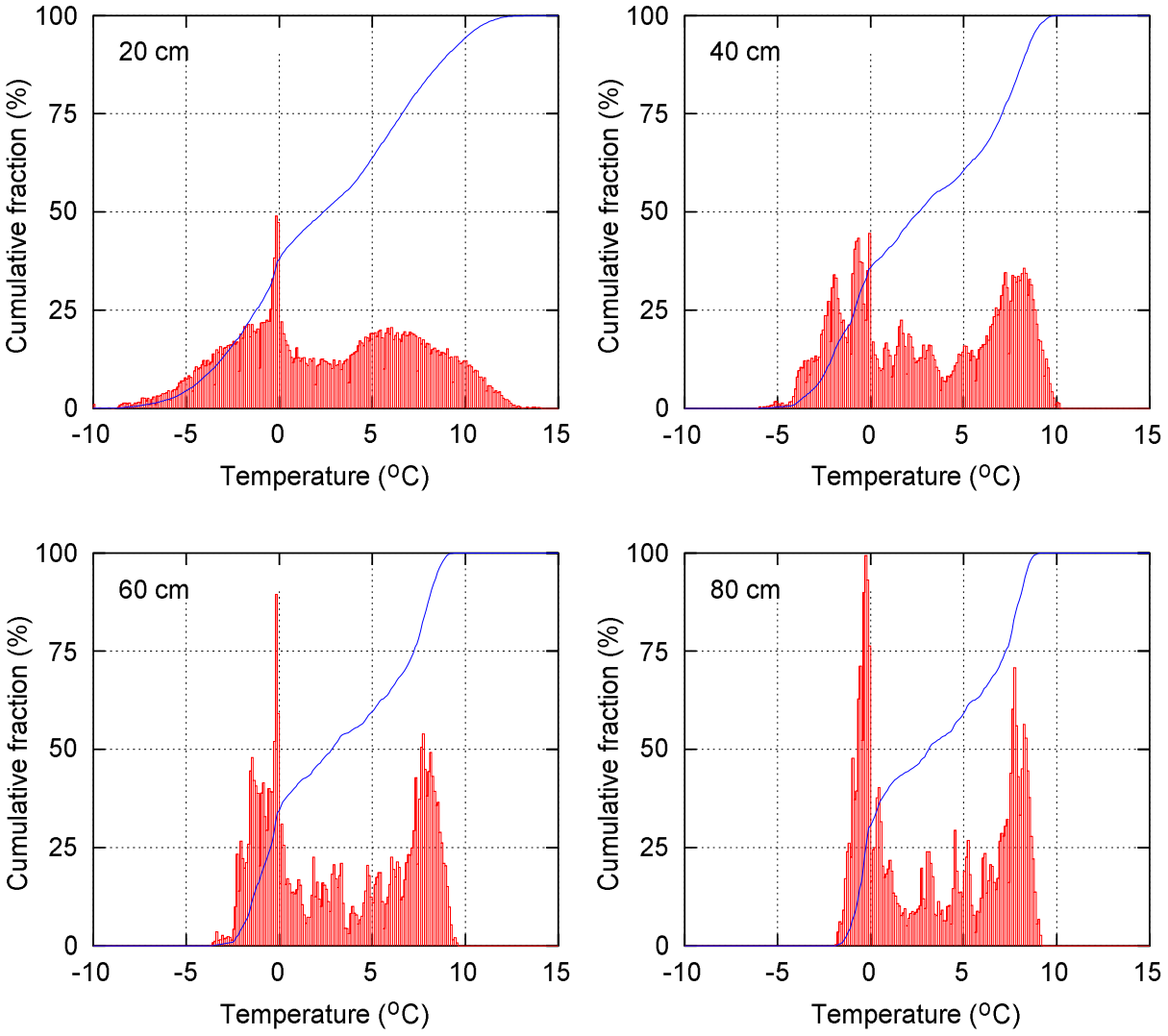

Figure 7: Cumulative distribution of subsurface temperatures at 20, 40, 60, and 80 cm during the period from 2000 April to 2002 March, overlaid on the corresponding histogram in arbitrary units.

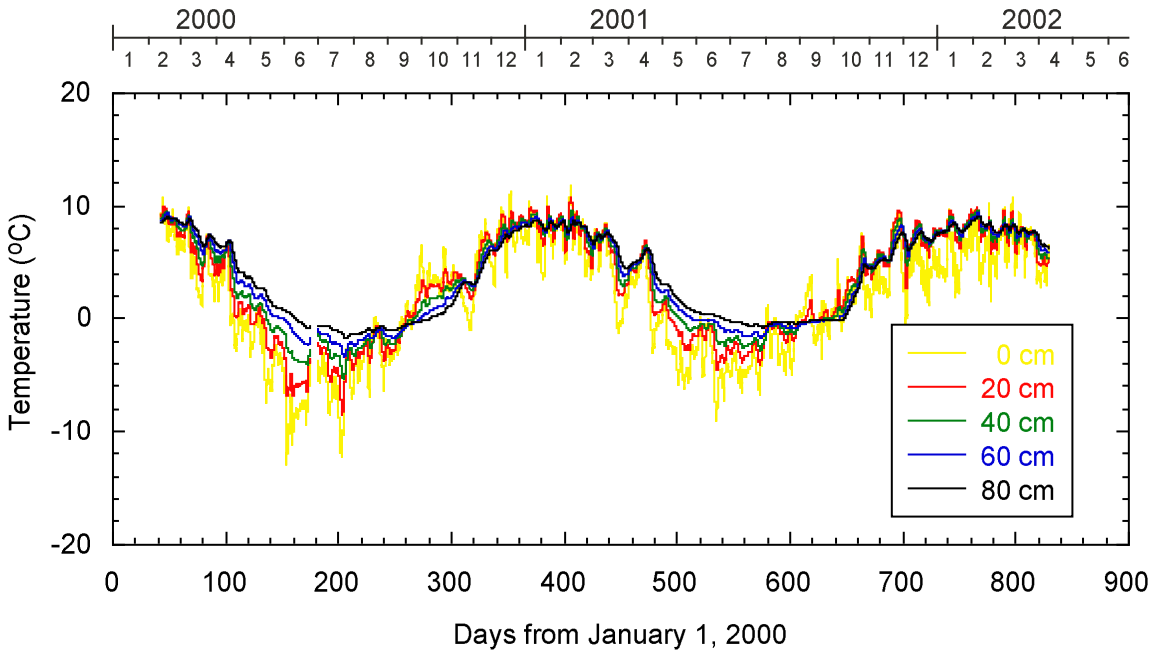

Figure 8: Mean daily temperature of subsurface layer at different depths (0, 20, 40, 60, and 80 cm).

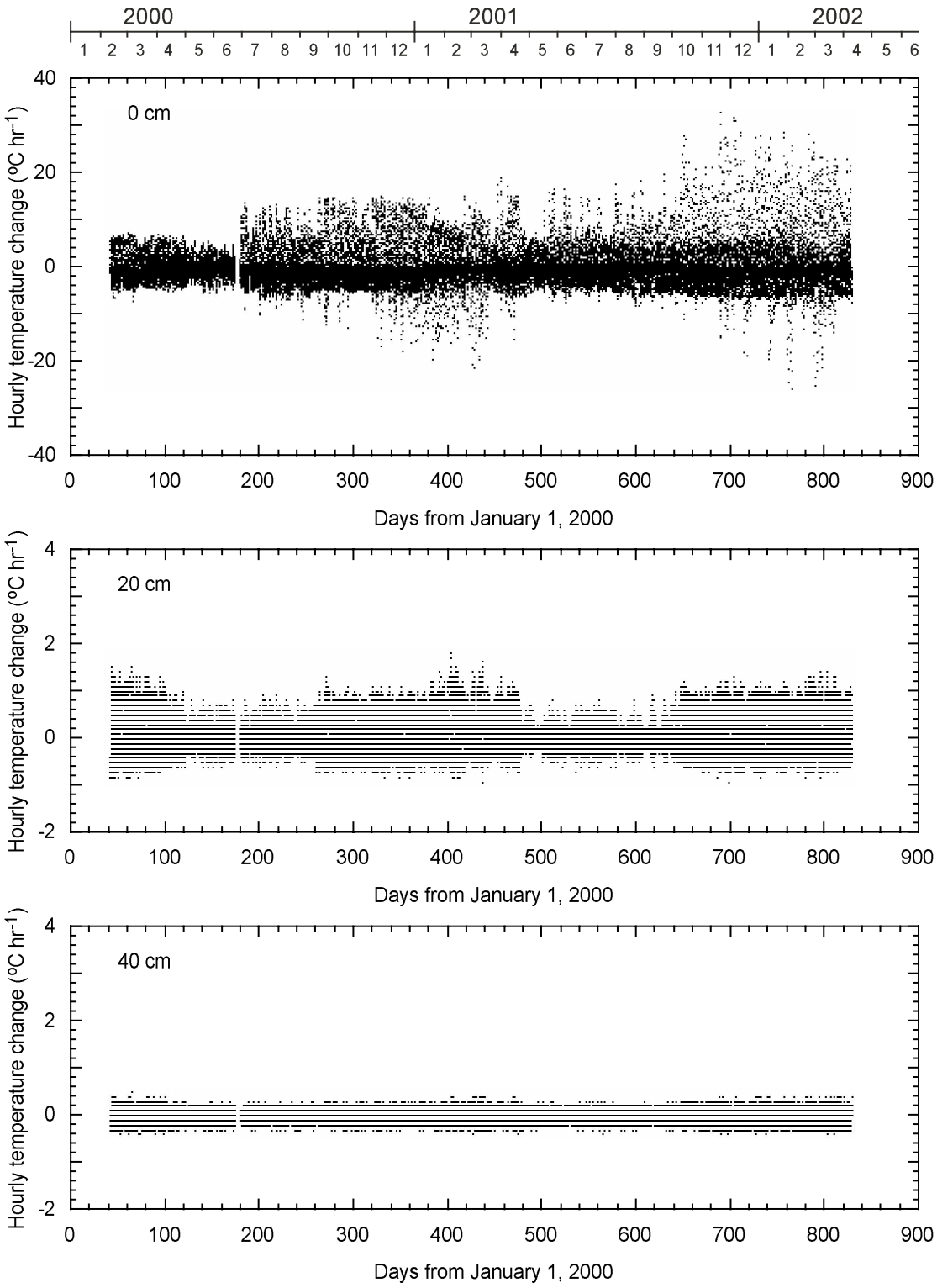

Figure 9: Hourly temperature changes in $^{\circ}\mathrm{C\,hr^{-1}}$ at different depths. Note change in scale of vertical axes. Also note that these values may be affected up to $0.2^{\circ}\mathrm{C\,hr^{-1}}$ due to the $0.1^{\circ}\mathrm{C}$ quantization of the readout.

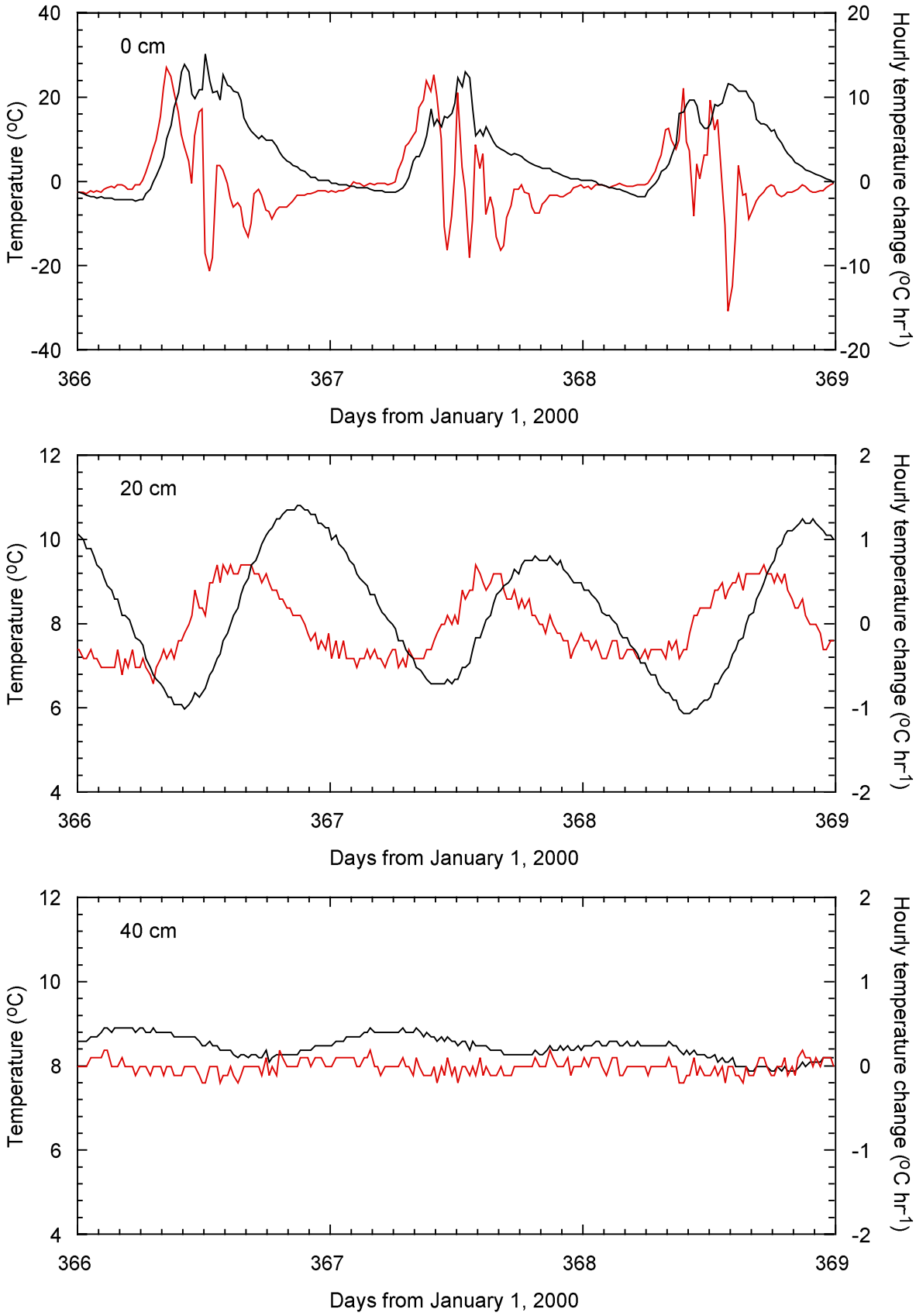

Figure 10: Temperature (*black*) and hourly temperature change (*red*) at 0, 20, and 40 cm as a function of time for the first three days of the year 2001. Note change in scale of vertical axes.

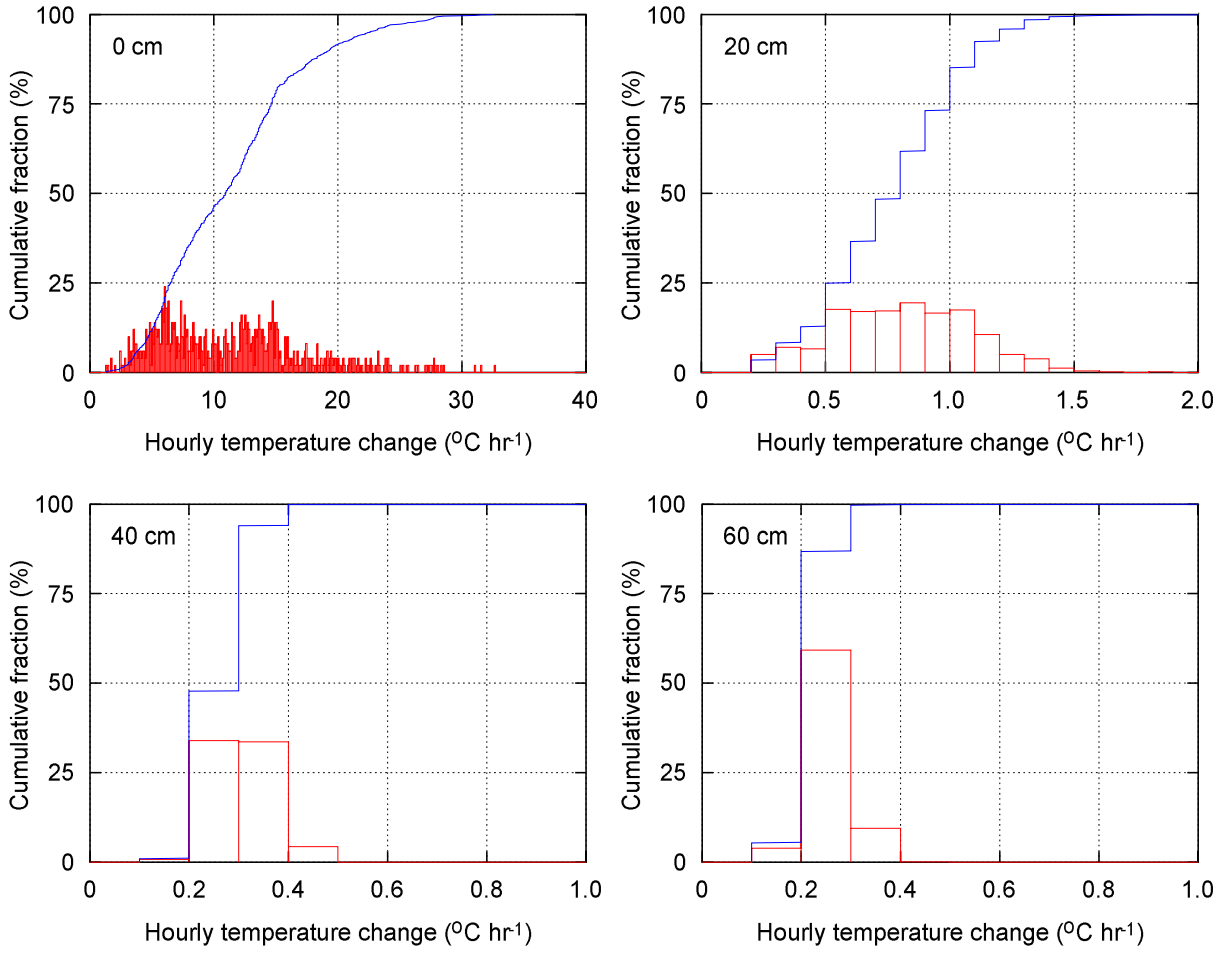

Figure 11: Cumulative distribution of the maximum hourly temperature change of the day in $^{\circ}\mathrm{C\,hr^{-1}}$ at 0, 20, 40, and 60 cm, overlaid on the corresponding histogram in arbitrary units. Note that the maximum value may be overestimated up to $0.2^{\circ}\mathrm{C\,hr^{-1}}$ due to the 0.1°C quantization of the readout. The plot for the 80 cm data has almost exactly the same appearance and thus the histogram shown as the 60 cm data actually illustrates the overestimation due to the quantization effect.

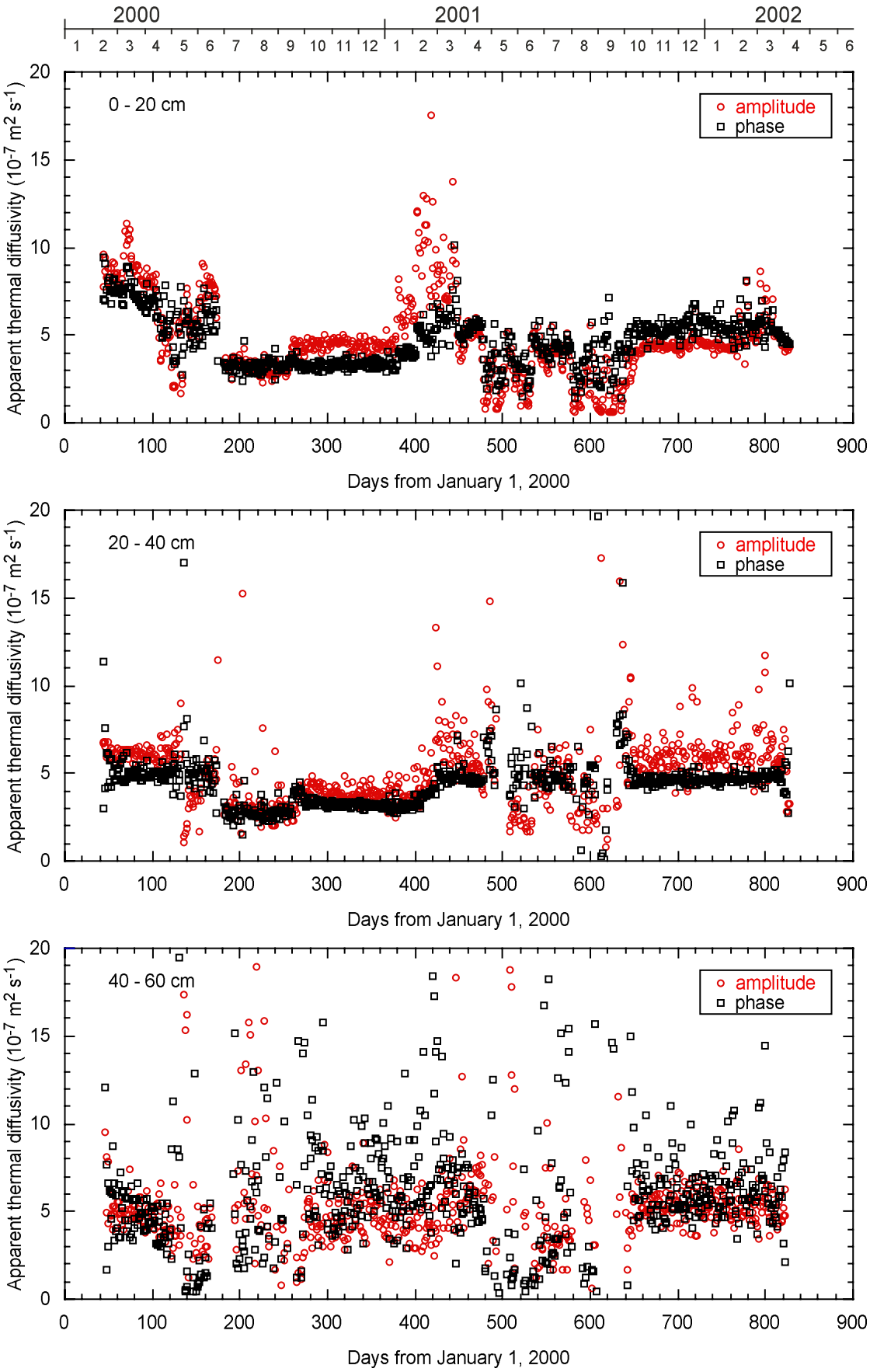

Figure 12: Variation of apparent thermal diffusivity calculated from the amplitude suppression and from the phase delay.

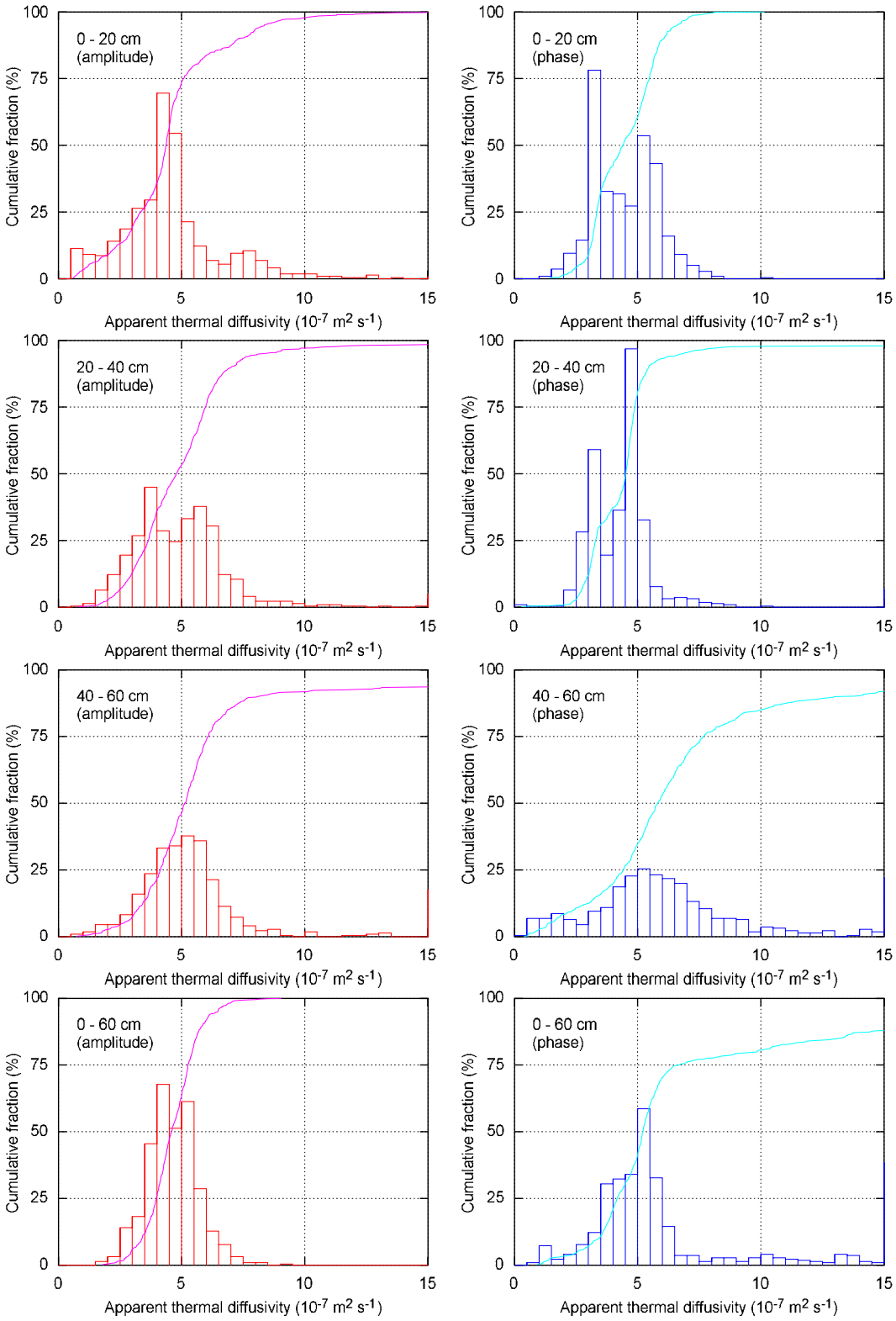

Figure 13: Cumulative distribution of apparent thermal diffusivity calculated from the amplitude suppression and from the phase delay, overlaid on the corresponding histogram in arbitrary units.